Stability of an emittance-dominated sheet-electron beam in planar wiggler and periodic permanent magnet structures with natural focusing

B. E. Carlsten, L. M. Earley, F. L. Krawczyk, and S. J. Russell
Los Alamos National Laboratory, Los Alamos, New Mexico, USA

J. M. Potter
JP Accelerator Works, Los Alamos, New Mexico, USA

P. Ferguson
MDS Company, Oakland, California, USA

S. Humphries, Jr.
Field Precision, Albuquerque, New Mexico, USA

(Received 1 November 2004; revised manuscript received 11 April 2005; published 29 June 2005; publisher error corrected 10 November 2005)

A sheet-beam traveling-wave amplifier has been proposed as a high-power generator of rf from 95 to 300 GHz, using a microfabricated rf slow-wave structure [Carlsten *et al.*, IEEE Trans. Plasma Sci. **33**, 85 (2005)], for emerging radar and communications applications. The planar geometry of microfabrication technologies matches well with the nearly planar geometry of a sheet beam, and the greater allowable beam current leads to high-peak power, high-average power, and wide bandwidths. Simulations of nominal designs using a vane-loaded waveguide as the slow-wave structure have indicated gains in excess of 1 dB/mm, with extraction efficiencies greater than 20% at 95 GHz with a 120-kV, 20-A electron beam. We have identified stable sheet-beam formation and transport as the key enabling technology for this type of device. In this paper, we describe sheet-beam transport, for both wiggler and periodic permanent magnet (PPM) magnetic field configurations, with natural (or single-plane) focusing. For emittance-dominated transport, the transverse equation of motion reduces to a Mathieu equation, and to a modified Mathieu equation for a space-charge dominated beam. The space-charge dominated beam has less beam envelope ripple than an emittance-dominated beam, but they have similar stability thresholds (defined by where the beam ripple continues to grow without bound along the transport line), consistent with the threshold predicted by the Mathieu equation. Design limits are derived for an emittance-dominated beam based on the Mathieu stability threshold. The increased beam envelope ripple for emittance-dominated transport may impact these design limits, for some transport requirements. The stability of transport in a wiggler field is additionally compromised by the beam's increased transverse motion. Stable sheet-beam transport with natural focusing is shown to be achievable for a 120-kV, 20-A, elliptical beam with a cross section of 1 cm by 0.5 mm, with both a PPM and a wiggler field, with magnetic field amplitude of about 2.5 kG.

DOI: 10.1103/PhysRevSTAB.8.062001 PACS numbers: 41.85.−p

I. INTRODUCTION

A new need for high-frequency, high-power rf sources has been emerging for advanced radar and communications, with frequencies in the band between 100 and 300 GHz and peak powers as high as several hundreds of kilowatts, and with bandwidths of up to 10%. After investigation of different high-frequency gain mechanisms including dielectric Cherenkov masers [1] and two-beam amplifiers, we determined that planar, microfabricated, traveling-wave tube (TWT) amplifiers could best satisfy the needs of these new missions [2]. This type of source consists of a very thin sheet-electron beam passing through a periodic slow-wave structure that could be either single or double sided [3]. We have focused our technical efforts on understanding the underlying physics and technology of the double-sided interaction and developing a demonstration experiment.

Earlier work [4] has identified the key enabling technologies as (i) the sheet-beam formation and transport and (ii) the rf mode control in the structure. (For our purposes, we use the term ''sheet beam'' to specifically refer to an elliptical beam with a high aspect ratio.) Our analytic and experimental program has focused on these two issues, mostly for the nominal parameters of a 20-A, 120-kV beam with elliptical cross section 1 cm by 0.5 mm, in a vane-loaded waveguide with period 0.5 mm and gap 0.75 mm, synchronous at 95 GHz.

Sheet-beam transport in either planar periodic permanent magnet (PPM) or wiggler structures has been shown to be resistant to the diocotron and other velocity shear instabilities [5,6], which disrupt sheet-beam transport in solenoidal fields. In addition, periodic magnetic structures, like wigglers and PPM stacks, built with permanent magnets, are significantly smaller and lighter weight than

conventional solenoid magnets. These considerations have motivated us to study the applicability of these types of permanent magnetic configurations for the transport of emittance-dominated sheet-electron beams. Previous work has also shown space-charge dominated beams in these structures to obey stability criteria associated with the Mathieu equation [7], similar to the case for cylindrical periodic permanent magnet (PPM) focusing [8]. However, little previous work has been done on effects that arise when the transport is emittance-dominated instead of space-charge dominated, particularly in regards to modifications to stability thresholds and beam envelope ripple, and that is the purpose of this paper. To understand the issues associated with stable sheet-beam transport for an emittance-dominated beam, analytic expressions are derived for the transverse beam dynamics for the case of ''natural focusing'' (focusing only in the beam's narrow direction) and confirmed with numerical simulations. We derive the envelope equation for sheet-beam focusing in periodic structures, including both emittance and space-charge effects, which leads to simple design formulas. Stability regions are found which agree with the stability bands of the Mathieu equation. Surprisingly, the beam envelope ripple even below the stability threshold is found to be significantly larger for an emittance-dominated beam than for a space-charge dominated beam.

In general, the magnetic field for a planar focusing array can be expressed as [6]

$$B = -\nabla \chi_m, \tag{1}$$

where

$$\chi_m = \frac{B_w}{k_z} \cosh(k_x x) \cos(k_z z)[a \sinh(k_y y) + b \cosh(k_y y)], \tag{2}$$

where k_z is 2π divided by the focusing period. The $\cosh(k_x x)$ term is typically introduced by shaping of the magnets or pole pieces. The wave equation relates the wave numbers, and gives $k_x^2 + k_y^2 = k_z^2$. Here we assume the beam motion is in $\hat{z}$, the beam is narrow in $\hat{y}$ and wide in $\hat{x}$. B_w is used to denote the peak field, to be consistent with previous work from the free-electron laser community. In Eq. (2), we use the parameters a and b to differentiate between a wiggler field ($a = 1, b = 0$) and a PPM field ($a = 0, b = 1$), which are the only two possibilities with planar symmetry. (Only the PPM field exists with cylindrical symmetry.) This potential gives us these field components:

$$\begin{aligned} B_x &= -\frac{k_x}{k_z} B_w \sinh(k_x x) \cos(k_z z)[a \sinh(k_y y) + b \cosh(k_y y)], \\ B_y &= -\frac{k_y}{k_z} B_w \cosh(k_x x) \cos(k_z z)[a \cosh(k_y y) + b \sinh(k_y y)], \\ B_z &= B_w \cosh(k_x x) \sin(k_z z)[a \sinh(k_y y) + b \cosh(k_y y)]. \end{aligned} \tag{3}$$

When $k_x = 0$, B_y and B_z are independent of horizontal position, and B_x vanishes. This leads to only focusing in the $\hat{y}$ plane, which in the free-electron laser community has been known as ''natural focusing.'' With $k_x \neq 0$, there is horizontal focusing of the beam in addition to vertical focusing, which is known as two-plane focusing. For real transport sections, some horizontal focusing will always be needed due to the space-charge fields of the beam, but for the type of sheet beam we are concerned with, the horizontal focusing required is over an order of magnitude smaller than the vertical focusing, and some key insights can be made into planar sheet-beam transport just considering natural focusing.

Our goal in this paper is to quantify the stability of natural focusing with both PPM and wiggler field configurations of emittance-dominated beams, space-charge dominated beams, and beams with both space-charge and emittance effects. This material is described in the following five sections. The following section, Sec. II, contains a review of the stability of cylindrical PPM focusing, which has been previously investigated in detail for the space-charge dominated case. This review material is included because new material in later sections relies heavily on the stability concepts of this well-known case. The transverse equation of motion for this type of focusing becomes a modified Mathieu equation, which still maintains the basic Mathieu equation's regions of stability. We analyze natural (single-plane) focusing of sheet beams in Sec. III, which leads to a transverse equation of motion very similar to the case for the cylindrical focusing case reviewed in Sec. II, resulting in a modified Mathieu equation. The transverse envelope equation is then derived in Sec. IV. The envelope equation is used to analyze the transverse equation of motion, and allows us to derive simple stability limit expressions for the maximum period of the focusing for a given transverse beam emittance and size, and conversely for the maximum transverse emittance given the period of the focusing. Simulations of natural focusing are presented in Sec. V verifying the envelope equation results, using a ray-tracing code. Stability of the natural focusing is analyzed using simulations in Sec. VI, for various cases of space-charge dominated, emittance-dominated, and mixed beams. We find that, in general, emittance-dominated beams have much greater envelope ripple than do space-charge dominated beams, but both their stability thresholds (in terms of field strength or focusing period) are about the same, and can be predicted by the Mathieu equation. In addition, the stability of wiggler-focused beams is degraded by about 25% due to the large transverse beam velocities.

II. REVIEW OF PERIODIC FOCUSING

In this section, we summarize the well-known analysis for cylindrical focusing of an cylindrical electron beam with periodic permanent magnet (PPM) focusing, de-

scribed by Mendel, Quate, and Yocum [8] (their motivation was to order to reduce the weight of a traveling-wave tube relative to a tube focused with an electromagnetic solenoid, which is important if the tube is to be used as a radar system in a plane). Cylindrical periodic focusing is well known, and has been used in microwave tubes for decades. The stability properties of the transport are well understood in relation to the transverse equation of motion, which is a modified Mathieu equation. We will extend this analysis in subsequent sections to emittance-dominated beams and to a planar geometry.

We start with assuming this form for the axial magnetic field:

$$B_z(z) = B_p \cos\left(\frac{2\pi z}{L}\right), \tag{4}$$

where B_p is the peak axial field on axis and L is the periodicity of the field profile. An electron's azimuthal velocity is given by the paraxial form of Busch's theorem (or conservation of canonical angular momentum) [9]:

$$\dot{\theta} = \frac{e}{2m\gamma}\left[-B_p \cos\left(\frac{2\pi z}{L}\right) + \frac{r_c^2}{r^2} B_c\right], \tag{5}$$

where B_c is the axial magnetic field at the cathode, r_c is the electron's radius on the cathode, m is the electronic mass, and γ is the relativistic mass factor. With no field on the cathode, the particle radial equation of motion becomes

$$\ddot{r} = \frac{I}{I_A}\frac{2c^2 r}{\beta\gamma^3 r_b^2}\left[1 - \frac{B_p^2}{B_{\mathrm{BR}}^2}\cos^2\left(\frac{2\pi z}{L}\right)\right], \tag{6}$$

where $I_A = 4\pi\varepsilon_0 mc^3/e$ (about 17 kA), r_b is the beam edge radius, and the Brillouin field B_{BR} is given by $B_{\mathrm{BR}} = (mc/er_b)\sqrt{8I/\beta\gamma I_A}$ [9]. The Brillouin field is the uniform field strength needed to provide balanced flow (for a space-charge dominated beam). Numeric calculations by Mendel *et al.* [8] showed a minimum beam ripple if $B_p = \sqrt{2}B_{\mathrm{BR}}$ (the same rms focusing strength as for the uniform focusing case).

This is often rewritten as

$$\frac{d^2 r}{dT^2} + \alpha[1 + \cos 2T]r - \tilde{\beta} r = 0, \tag{7}$$

with $T = 2\pi z/L$, $\alpha = [L^2/(2\pi)^2](I/I_A) \times (B_p^2/\beta^3\gamma^3 r_b^2 B_{\mathrm{BR}}^2) = [L^2/(2\pi)^2](e^2 B_p^2/\beta^2\gamma^2 8m^2c^2)$ (note that α is independent of beam current and only a function of the focusing parameters) and $\tilde{\beta} = 2[L^2/(2\pi)^2 r_b^2] \times (I/I_A)(1/\beta^3\gamma^3)$, which represents the space-charge force. If the flow is approximately balanced and the beam envelope is mostly constant (in other words, r_b is mostly independent of T), then $\tilde{\beta}$ is a constant of the motion (α is independent of r_b and always a constant of the motion). Also for mostly balanced flow for a laminar (space-charge dominated) beam, the $\cos 2T$ term will average to zero and we have $(d^2 r_b/dT^2) + \alpha r_b - \tilde{\beta} r_b = 0$ for the edge of the beam, which has a balanced flow solution if $\alpha = \tilde{\beta}$, which is equivalent to Mendel's balance condition $2B_{\mathrm{BR}}^2 = B_p^2$. In the emittance-dominated regime, where space charge can be neglected, the equivalent single-particle equation of motion can be written as

$$\frac{d^2 r}{dT^2} + \alpha[1 + \cos 2T]r = 0, \tag{8}$$

which is recognized as a Mathieu equation. In this limit, we can picture the beam as a collection of intersecting trajectories, and that no single trajectory overlaps the beam edge for more than a short time.

In both limits, the transport can be unstable if $\alpha > 0.66$. For the emittance-dominated limit, it is well known that the solution to the Mathieu equation is stable if $\alpha < 0.66$ or $1.72 < \alpha < 3.76$ or $\alpha > 6.10$. Surprisingly, in the space-charge limit, when $\alpha \approx \tilde{\beta}$, roughly the same stability threshold is found [7,8].

If we write a plasma wavelength λ_p as $\lambda_p = 2\pi v_z/\omega_p$, where ω_p is the beam's plasma frequency, the lowest order stability criteria for a space-charge dominated beam can be rewritten as

$$\lambda_p > 1.15L. \tag{9}$$

In the microwave tube literature, λ_p/L is sometimes called the "beam stiffness factor."

The Mathieu stability criteria arises from the thin lens focusing stability. We can see this by thinking of the PPM field as a series of thin lenses, separated by a distance $L/2$ [10]. Ignoring space charge, the radial equation of motion inside the lenses is [from Eq. (6)]

$$r'' = -\frac{rB_p^2 e^2}{4\beta^2\gamma^2 m^2 c^2}\cos^2\left(\frac{2\pi z}{L}\right). \tag{10}$$

We consider the lens' focal length as $(1/f) = (\Delta r'/r)$, which we calculate by direct integration (here we assume the particle radius is not changing much over the length of the lens— this approximation is poor for the case the focusing is nearly unstable, but still gives a surprisingly accurate result):

$$\frac{1}{f} = \frac{B_p^2 e^2}{4\beta^2\gamma^2 m^2 c^2}\int_{-L/4}^{L/4}\cos^2\left(\frac{2\pi z}{L}\right)dz = \frac{B_p^2 e^2}{4\beta^2\gamma^2 m^2 c^2}\frac{L}{4}, \tag{11}$$

which must be less than $8/L$ for stability (from simple ray tracing), which gives the discrete lens stability criteria as

$$\frac{B_p^2 e^2}{4\beta^2\gamma^2 m^2 c^2}\frac{L^2}{32} < 1. \tag{12}$$

Written this way, the Mathieu stability equation looks like

$$\frac{B_p^2 e^2}{4\beta^2\gamma^2 m^2 c^2}\frac{L^2}{8\pi^2} < 0.66 \tag{13}$$

and we see the thin lens analysis is actually pretty good (the Mathieu stability criteria leads to a lens period of about 0.75 times the thin lens minimum period). Hence, we can interpret the stability criteria more-or-less as the simple ray-tracing stability of lenses.

III. SINGLE-PLANE FOCUSING OF SHEET BEAMS (NATURAL FOCUSING)

In this section, we derive the equivalent single-particle equation of motion [Eq. (8)] for the planar case, following Booske *et al.* [5,6]. We point out that without horizontal focusing the analysis is simplified by the existence of a conserved canonical horizontal momentum. The nonzero magnetic field elements for natural focusing are

$$B_z(y, z) = B_w[a\sinh(k_w y) + b\cosh(k_w y)]\cos(k_w z),$$
$$B_y(y, z) = B_w[a\cosh(k_w y) + b\sinh(k_w y)]\sin(k_w z), \tag{14}$$

where here k_w is 2π divided by the focusing period and as before we use the parameters a and b to differentiate between a wiggler field ($a = 1, b = 0$) and a PPM field ($a = 0, b = 1$). This field is generated by the vector potential

$$A_x(y, z) = -\frac{B_w}{k_w}[a\cosh(k_w y) + b\sinh(k_w y)]\cos(k_w z). \tag{15}$$

There is no space-charge force in $\hat{x}$ if we consider an infinitely wide beam, and then

$$\gamma m\frac{d}{dt}\dot{x} = e(\dot{y}B_z - \dot{z}B_y) = e\left(-\dot{y}\frac{\partial}{\partial y}A_x - \dot{z}\frac{\partial}{\partial z}A_x\right) = -e\frac{d}{dt}A_x, \tag{16}$$

leads to

$$\Delta(\gamma\dot{x}) = -\frac{e}{m}\Delta A_x, \tag{17}$$

which is the planar version of Busch's theorem (the conservation of canonical angular momentum with cylindrical symmetry).

If there is no field on the cathode and no initial horizontal motion [using $-(\partial/\partial y)A_x = B_z$]

$$\dot{x} = \frac{e}{m\gamma}\int_0^y B_z dy \tag{18}$$

or

$$\dot{x} = -\frac{e}{m\gamma}A_x = \frac{e}{m\gamma}\frac{B_w}{k_w}[a\cosh(k_w y) + b\sinh(k_w y)]\cos(k_w z). \tag{19}$$

Using $\ddot{y} = (e/m\gamma)(v_z B_x - v_x B_z)$ + space charge force, we have

$$\ddot{y} = \left(\frac{e}{m\gamma}\right)^2\frac{B_w^2}{k_w}[a\cosh(k_w y) + b\sinh(k_w y)][a\sinh(k_w y) + b\cosh(k_w y)]\cos^2(k_w z) + \text{space charge force}. \tag{20}$$

For a uniformly filled ellipse, the space-charge force is proportional to y. For small y, $\cosh(k_w y) = 1$ and $\sinh(k_w y) = k_w y$, and if $a = 1, b = 0$ or $a = 0, b = 1$, we end up with linear focusing in y and recover the same modified Mathieu equation from the previous section. For a mix of nonzero a and b, we need to numerically demonstrate that the force is sufficiently linear as to prevent any emittance growth, which we do in Sec. V. For emittance-dominated transport, the space-charge force can be neglected altogether, and we recover the Mathieu equation

$$\ddot{y} + y\left(\frac{e}{m\gamma}\right)^2 B_w^2\cos^2(k_w z)(a + b) = 0, \tag{21}$$

where now the Mathieu parameter α is given by

$$\alpha = \frac{B_w^2}{2}\left(\frac{e}{mc\gamma\beta}\right)^2\left(\frac{L}{2\pi}\right)^2. \tag{22}$$

There is an additional feature of wiggler focusing that needs to be recognized. For small amplitude motion, the transverse motion in a wiggler field is

$$\dot{x} = \frac{e}{m\gamma}\frac{B_w}{k_w}\cos(k_w z) \qquad \text{(wiggler only)}, \tag{23}$$

which is a maximum at $z = n\pi/k_w$, with amplitude $v_{x,\max} = (e/m\gamma)(B_w/k_w)$. This transverse motion cannot exceed the total velocity of the beam, βc [6]. This results in the inequality

$$B_w^2\left(\frac{e}{mc\gamma\beta}\right)^2\left(\frac{L}{2\pi}\right)^2 < 1 \qquad \text{(wiggler only)}. \tag{24}$$

Comparing this to Eq. (22) for the Mathieu parameter α, where the quantity on the left-hand side must be less than 1.32, this requirement puts about a 15% stricter limit on the applied magnetic field or period of the focusing.

More importantly, though, this feature (large-order horizontal motion) leads to greater degradation of the transport before the stability limit (we will see this in the stability simulations in Sec. V). The derivation for the vertical equation of motion earlier in this section used the paraxial approximation that the axial motion was independent of the transverse motion, which, for the wiggler geometry fails as the limit in Eq. (24) is approached. (In particular, the relationship between d/dz and d/dt was assumed to be independent of z.)

Even though this analysis predicts that the wiggler configuration has more limited stability than the PPM configuration, it is still preferable for some regimes. In PPM

focusing, the beam's vertical motion is of higher order than in wiggler focusing, which could cause added beam interception. This larger vertical motion can also lead to significant emittance growth, for high aspect-ratio beams.

IV. BEAM ENVELOPE EVOLUTION WITH NATURAL FOCUSING

In this section, we derive the envelope equation for the edge of an elliptical beam, with both space-charge and emittance effects. After finding the balance condition for a beam in the emittance-dominated regime, we develop relations between the required wiggler/PPM peak field strength and beam emittance, and limitations on the period length to maintain orbit stability.

Now let us consider the average focusing force where the betatron period, or focal length, is long compared to the wiggle period,

$$\ddot{y} = -y\frac{B_w^2}{2}\left(\frac{e}{m\gamma}\right)^2 = -yK\beta^2c^2, \tag{25}$$

where we have introduced a focusing wave number K. Sheet beams are unusual—most microwave tubes operate strictly in the space-charge dominated regime. However, sheet beams can operate in both the space-charge and emittance regimes because of the large differences in the horizontal and vertical beam sizes. We will show this for the practical example of the Los Alamos experiment [11] at 120 kV, with a 20 A beam with a transverse cross section of 10 mm by 0.5 mm.

We will start by deriving the sheet-beam envelope equation, and then use the average focusing force, beam emittance, and space-charge force to define matched flow (where the envelope is matched in an rms sense). We will define rms beam sizes as

$$X = \langle x^2\rangle^{1/2}, \qquad Y = \langle y^2\rangle^{1/2}. \tag{26}$$

We will take the axial derivatives of Y to get the vertical envelope equation—to get the X envelope equation, just substitute X for Y. Starting with $Y^2 = \langle y^2\rangle$, we take an axial derivative to get $2YY' = \langle 2yy'\rangle$ or $YY' = \langle yy'\rangle$, which gives us $Y' = \langle yy'\rangle/Y$. A second axial derivative yields $YY'' + Y'^2 = \langle yy''\rangle + \langle y'^2\rangle$, or $Y'' = -(Y'^2/Y) + [(\langle yy''\rangle + \langle y'^2\rangle)/Y] = (\langle yy''\rangle/Y) + [(\langle y^2\rangle\langle y'^2\rangle)/Y^3] - (\langle yy'\rangle^2/Y^3)$, which can be rewritten as

$$Y'' = \frac{\langle yy''\rangle}{Y} + \frac{\varepsilon_y^2}{Y^3}, \tag{27}$$

where $\varepsilon_y^2 = \langle y^2\rangle\langle y'^2\rangle - \langle yy'\rangle^2$ is the square of the unnormalized emittance.

Next, we will find the force term. Lawson's approximate form for the space-charge field for an elliptical beam is [12]

$$E_x = \frac{m}{e}\left(\frac{e\rho}{\varepsilon_0 m}\right)\frac{Y}{X+Y}x, \qquad E_y = \frac{m}{e}\left(\frac{e\rho}{\varepsilon_0 m}\right)\frac{X}{X+Y}y, \tag{28}$$

where ρ is the uniform density of the ellipse. Together, the focusing and space-charge terms lead to (for a laminar, quasilaminar, or emittance-matched uniform density beam):

$$\begin{aligned}\ddot{y} &= -y\frac{B_w^2}{2}\left(\frac{e}{m\gamma}\right)^2 + y\frac{e\rho}{\gamma^3 m\varepsilon_0}\frac{X}{X+Y} \\ &= -yK\beta^2c^2 + y\frac{eI}{\gamma^3 m\pi(4XY)\beta c\varepsilon_0}\frac{X}{X+Y},\end{aligned} \tag{29}$$

where we have used the definition of the focusing wave number K and the $(4XY)$ is the product of the ellipse major and minor axes. Also note for a paraxial beam

$$y'' = \frac{d^2y}{dz^2} = \frac{d}{dz}\left(\frac{dy}{dz}\right) = \frac{dt}{dz}\frac{d}{dt}\left(\frac{dt}{dz}\frac{dy}{dt}\right) = \frac{\ddot{y}}{\beta^2c^2}. \tag{30}$$

This leads to

$$\begin{aligned}\frac{\langle yy''\rangle}{Y} &= \frac{\langle y^2\rangle}{Y}\left(-K + \frac{eI}{\gamma^3 m\pi(4XY)\beta^3c^3\varepsilon_0}\frac{X}{X+Y}\right) \\ &= Y\left(-K + \frac{I/I_A}{XY\gamma^3\beta^3}\frac{X}{X+Y}\right)\end{aligned} \tag{31}$$

and the envelope equation becomes

$$Y'' = -Y\left(\frac{e}{\beta cm\gamma}\right)^2\frac{B_w^2}{2} + \frac{I/I_A}{\gamma^3\beta^3}\frac{1}{X+Y} + \frac{\varepsilon_{y,\mathrm{norm}}^2}{Y^3\gamma^2\beta^2}, \tag{32}$$

where the normalized vertical emittance $\varepsilon_{y,\mathrm{norm}}$ is defined in terms of the unnormalized vertical emittance as $\varepsilon_{y,\mathrm{norm}} = \beta\gamma\varepsilon_y$. We can identify the first term on the right hand side as a focusing term, the second term as a space-charge term, and the third term as an emittance term. At 120 kV, γ is 1.235 and $\gamma\beta$ is 0.724, and for the nominal Los Alamos design [11], the normalized beam emittance is 1.35 μm and the current is 20 A. For a 10 mm by 0.5 mm beam, Y is 0.125 mm and X is 2.5 mm, the focusing term is 40.9 m^{-1} times B_w^2 in tesla, the space-charge term is 1.18 m^{-1} (both horizontal and vertical envelope equation), and the emittance term is 1.79 m^{-1} (and 8.9×10^{-4} m^{-1} for the horizontal envelope equation).

The required focusing strength for these parameters is 0.266 T. With just the emittance (ignoring the space-charge force), the magnetic field strength would need to be 0.206 T, and with just the space-charge force, the magnetic field strength would need to be 0.168 T. We will compare these numbers to simulation results in later sections. Summarizing the nominal Los Alamos parameters, the natural focusing in the vertical plane mostly counteracts the defocusing effect of the beam emittance. The beam can be thought as horizontally laminar and vertically emittance dominated, but matched, resulting in a constant beam size.

Even for this low emittance, the emittance term dominates in the vertical dimension (and is negligible in the horizontal dimension). This transverse asymmetry is unique for sheet beams, and would be more pronounced for larger emittance cases. From a matched focusing point of view, the effect on the envelope is the same if the defocusing is emittance dominated or space-charge dominated. However, the single-particle equations of motion are different for the two cases. A space-charge dominated beam will have laminar flow, whereas an emittance-dominated beam will look like a collection of oscillating orbits out of phase filling the beam envelope. We should expect some differences in the stability behavior of these different types of flow. Specifically, space-charge defocusing modifies the single-particle equation of motion from the Mathieu equation, whereas the emittance, which has no influence on single-particle motion, does not.

The envelope equation establishes a relationship between the applied magnetic field and the emittance for balanced flow. For an emittance-dominated beam, we know the stability limit is given when the Mathieu parameter α, given in Eq. (22), reaches 0.66. Through these two relations, we can develop some design limits about stable transport of an emittance-dominated beam. Equating the focusing part of the envelope equation to the emittance part, we find that the required peak field is given by

$$B_{\mathrm{req}} = \sqrt{2}\varepsilon_{y,\mathrm{norm}}\frac{mc}{Y^2 e}. \tag{33}$$

Note that the required field only depends on the beam's normalized emittance and size, and not on beam energy.

Relating the field to the Mathieu parameter α, Eq. (22) we find

$$\alpha = \frac{\varepsilon_{y,\mathrm{norm}}^2}{\gamma^2\beta^2}\frac{1}{Y^4}\left(\frac{L}{2\pi}\right)^2. \tag{34}$$

Recalling that α must be less than 0.66, this puts a relation between the beam emittance, focusing period, and beam width.

The maximum allowable focusing period given the beam emittance and size is then

$$L_{\mathrm{max}} = 2\pi\sqrt{0.66}\frac{\gamma\beta}{\varepsilon_{y,\mathrm{norm}}}Y^2, \tag{35}$$

and the maximum allowable beam emittance given the focusing period and beam size is then

$$\varepsilon_{y\,\mathrm{max,norm}} = 2\pi\sqrt{0.66}\frac{\gamma\beta}{L}Y^2. \tag{36}$$

Using the beam size requirement for good coupling, these expressions, specifically for the planar TWT design, become, in terms of the free-space rf wavelength λ (using the approximation $Y = \lambda/24$),

$$L_{\mathrm{max}} = 2\pi\sqrt{0.66}\frac{\gamma\beta}{\varepsilon_{y,\mathrm{norm}}}\frac{\lambda^2}{(24)^2} \tag{37}$$

and

$$\varepsilon_{y\,\mathrm{max,norm}} = 2\pi\sqrt{0.66}\frac{\gamma\beta}{L}\frac{\lambda^2}{(24)^2} \tag{38}$$

which tell us that the normalized beam emittance must decrease as the frequency is increased, as there are physical limitations as to how small permanent magnets can be fabricated. For the above experimental parameters (λ is about 3 mm and the beam is at 120 kV), the maximum period is 4.27 cm for a normalized emittance of 1.35 μm (ignoring space charge). Conversely, the maximum normalized emittance is 5.7 μm for a period of 1 cm.

For a frequency of 300 GHz, the maximum allowable period for a normalized emittance of 1.4 μm is 0.46 cm, and the maximum allowable normalized emittance for a period of 1 cm is 0.64 mm. For current magnet technology, the beam emittance must be cooled if we want to build a 300 GHz tube. Also note from Eq. (33) that the required magnetic field for confinement, for a given emittance, scales as the frequency squared (because of the decrease in structure size and hence Y).

V. SIMULATIONS OF NATURAL FOCUSING

In this section, we will verify the predictions of the previous section for balanced envelope transport with natural focusing for the nominal Los Alamos sheet-beam experiment parameters, which are an elliptical electron beam of 20 A at 120 keV, with a cross section of 0.5 mm by 1 cm. The normalized emittance is 1.35 μm, and the beam is focused in a wiggler transport section. For proper injection in to the wiggler field in the following simulations, the beam horizontal motion is initially assumed to be

$$\dot{x} = -\frac{e}{\gamma m k_w}B_w\cos(k_w z)[a\cosh(k_w y) + b\sinh(k_w y)], \tag{39}$$

which is the condition from the conservation of canonical horizontal momentum. Although the single-particle angular momentum is no longer preserved in the presence of space-charge forces, this is still the condition for proper injection into the wiggler field, and should be provided by the tapering condition into the wiggler.

We used two codes to model this transport. Most of the following simulations are with the 3-dimensional ray-tracing code PUSHER [13], which uses the exact focusing field profiles, but an approximate space-charge field. Also, since natural focusing is a two-dimensional effect, we used the 2½-dimensional particle-in-cell (PIC) code TUBE [1] to model the transport. The application of a 2½-dimensional numerical model to this geometry required a parameter reduction of the distribution with which the beam was initialized [13].

PUSHER uses the ideal wiggler/PPM field for the external magnetic field and the Lawson form for the space-charge field (for a uniform-density elliptical cross-section beam), Eqs. (29). This form clearly satisfies Poisson's equation (in fact for any X and Y). The corresponding potential is

$$\phi = -\frac{\rho}{2\varepsilon_0}\frac{Yx^2 + Xy^2}{X + Y} + C, \tag{40}$$

where X and Y are specified by the boundary conditions on the beam pipe and C is an arbitrary constant. Note that if the elliptical beam is surrounded by a beam pipe at a given potential, the correct potential is given if $Y = y_{\max}^2$ and $X = x_{\max}^2$ (or alternatively $Y = 1/x_{\max}^2$ and $X = 1/y_{\max}^2$). For a large aspect ratio, the actual forms of X and Y do not matter much for the vertical force, because X will always be much larger than Y.

For this two scale problem (resolving both the details of the short-period magnetic profile and the long-period betatron focusing), PUSHER uses a new type of pushing routine, explicitly conserving energy from the magnetic field forces. The forces from the electric and magnetic fields are calculated separately. The effect from the electric field is calculated first. Then, the coordinate system is rotated so the net magnetic field on a given particle is only in the new axial direction. Then the motion from the magnetic field during the time step is found exactly, as the motion is easily described by a spiral about the net magnetic field. Finally, the coordinate system is unrotated to the original (x, y, z) frame. The advantage of this routine is that it exactly conserves energy from the magnetic field force, and does not lead to any numerical errors that accumulate. This routine very stable, allowing for greater spatial steps, and as a result is faster than a simple Boris push [14] or even the spatial-stepping Boris push [15], which are both accurate to only second order in spatial step.

Overall, the PUSHER simulations showed excellent agreement with the envelope equation. The nominal parameters led to a well focused beam, with minimal vertical size variations. Also, mixing in even as much as 10% PPM field with the wiggler field did not lead to any significant emittance increase, which is an important result because it quantifies the effect of losing linearity in the transverse equation of motion, Eq. (20). The nominal parameter simulation and some variations are shown below. The small beam size and the natural focusing is in the vertical (y) direction, and the wide beam size is in the horizontal (x) direction.

With only natural focusing and a peak magnetic field of 0.266 T, the beam expands significantly in the horizontal direction because of the horizontal space-charge force, also affecting the focusing in the vertical direction, Fig. 1. This expansion could be controlled by including two-plane focusing, but, for the purposes of numerically investigating just single-plane focusing, we numerically "turned off" the horizontal space-charge force for the rest of the single-plane focusing simulations reported in this paper. (The nonzero horizontal emittance was kept in the following simulations, but due to its small effect, it did not lead to any appreciable horizontal beam growth.) The added effects of two-plane focusing on transport stability are reported elsewhere [16]. In these and the following figures, 4 times the rms beam size is plotted, for both the vertical and horizontal dimensions, because this equals the full beam size for a hard-edged, uniform-density beam in both the space-charge and emittance-dominated regimes, and is a good measure of effective beam size for a nonuniform-density beam.

In the next set of figures (Fig. 2), we plot the vertical beam size, vertical emittance, horizontal beam size, and horizontal emittance as a function of the axial distance along the transport, for a total of 10 cm, with just the effect of the beam emittance and assuming zero beam current, and with a wiggler magnetic field

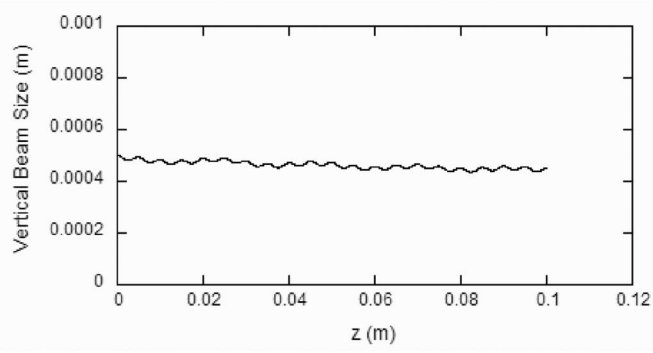

(a)

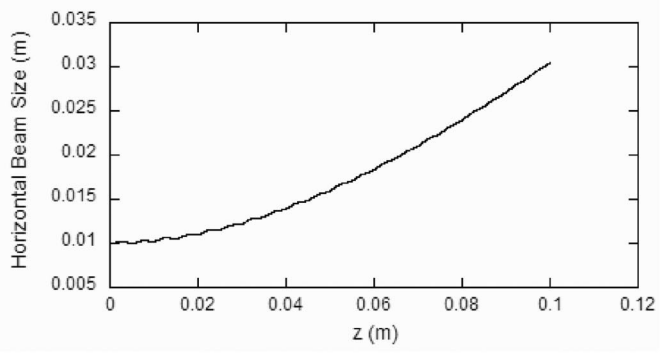

(b)

FIG. 1. (a) Vertical beam size, for the nominal natural focusing case (normalized emittance of 1.4 mm, 20 A, 0.266 T wiggler focusing field). (b) Horizontal beam size.

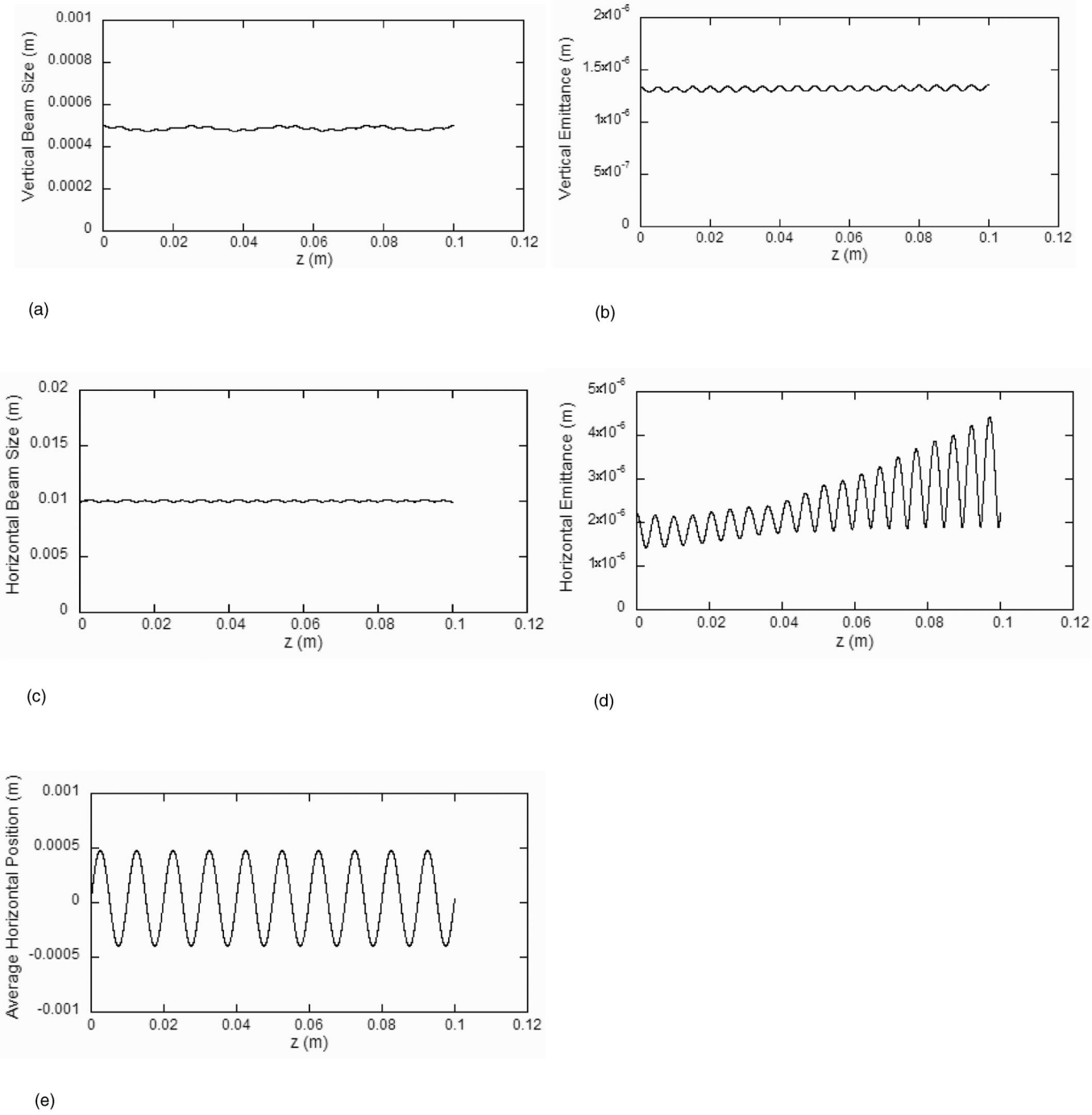

FIG. 2. Nominal PUSHER simulation of wiggler transport for the case with no space-charge, and transverse normalized emittances of 1.4 mm. (a) Vertical beam size versus axial distance. (b) Normalized vertical emittance fluctuation during the transport. (c) Horizontal beam size versus axial distance. (d) Normalized horizontal emittance fluctuation during the transport. (e) Average horizontal position of the beam, showing the clear horizontal ''wiggling'' of the beam.

with a peak field of 0.209 T. There is some initial mismatch of the beam, leading to a slight breathing of the rms beam size and average beam position, but the simulations confirm the numeric values predicted from the envelope equation in the previous section (a required focusing field of 0.206 T). The horizontal wiggling of the beam centroid is also shown, in Fig. 2(e).

In Fig. 3, we compare the transport with the equivalent PPM field. The beam transport is essentially identical to the wiggler transport, confirming the equivalent focusing strength of PPM and wiggler configurations.

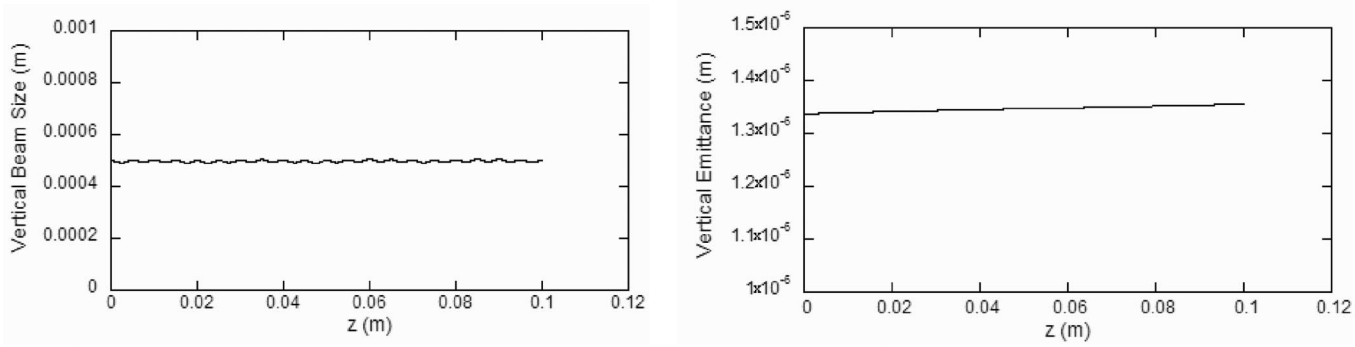

(a) (b)

FIG. 3. (a) 4-times y_{rms} beam size versus axial distance for the nominal PPM transport. (b) Normalized vertical emittance versus axial distance for the nominal PPM transport.

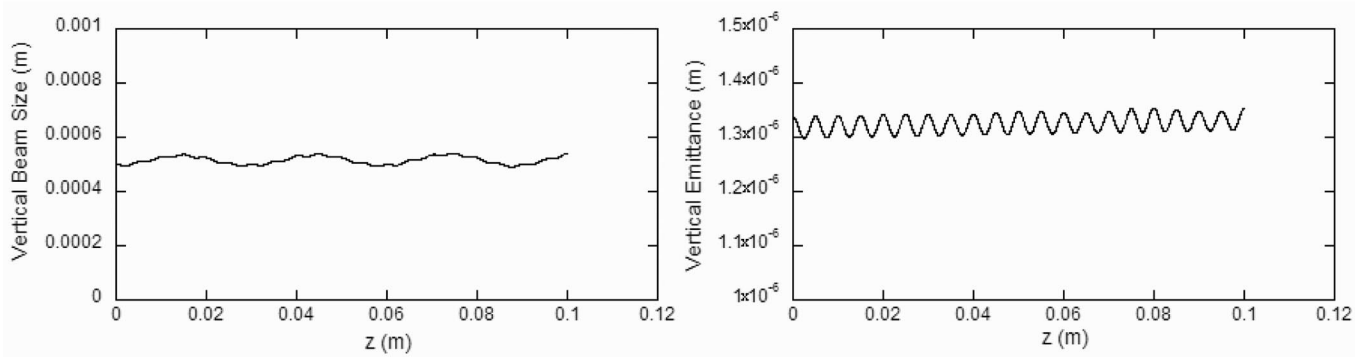

(a) (b)

FIG. 4. (a) 4-times y_{rms} beam size versus axial distance for a 90% wiggler, 10% PPM field split. (b) Normalized vertical emittance versus axial distance.

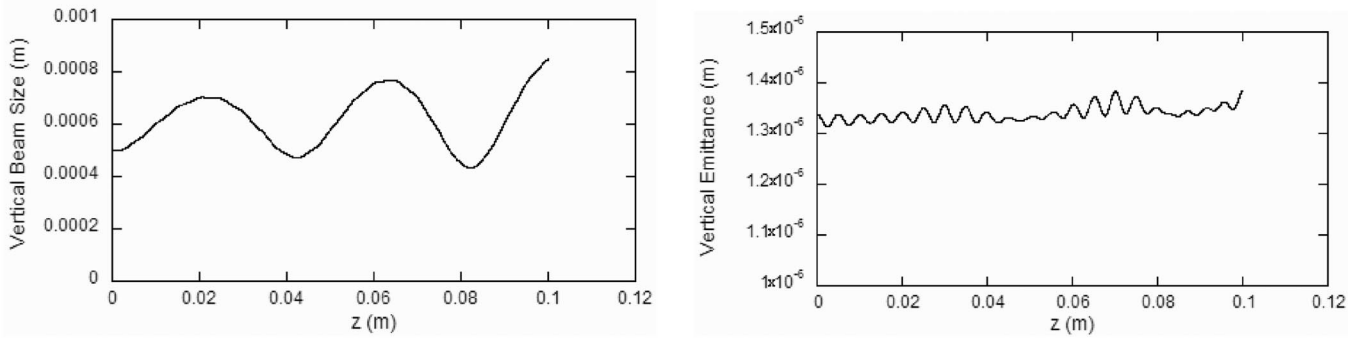

(a) (b)

FIG. 5. (a) 4-times y_{rms} beam size versus axial distance for a 70% wiggler, 30% PPM field split. (b) Normalized vertical emittance versus axial distance.

In Figs. 4 and 5 we study the effect of field configuration mixing. We anticipate from Eq. (20) that a mixture of the field configurations will lead to nonlinear focusing and emittance growth in the vertical plane. In Fig. 4, we plot the vertical beam width and emittance, for a 90% wiggler field and a 10% PPM field mixture (with $B_w = 2.5$ kG). In Fig. 5, we plot the same quantities for a 70% wiggler field and 30% PPM field mixture. We see that a 10% field error

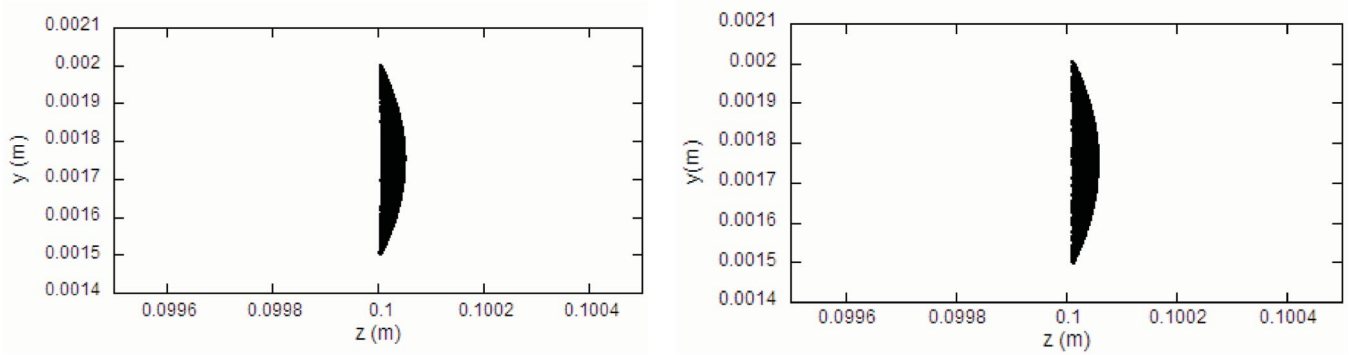

FIG. 6. Particle axial positions for an initially vertical slice of the beam, showing very small relative axial motion (a) for the wiggler field configuration, and (b) for the PPM field configuration.

does not appreciably degrade the transport, whereas a 30% error does. The 30% mixing is essentially at the boundary of the envelope evolution becoming unstable, because this field split does not provide enough natural focusing (but, surprisingly, the vertical emittance is still not affected). Note that the superposition of equal PPM and wiggler fields will cancel the magnetic field from one-half of the magnet array, and that loss of confinement will result. The opposition between the fields is consistent with these transport calculations.

We would anticipate from the greater transverse motion in a wiggler field configuration, that there may be more slippage than from a PPM field configuration. In Fig. 6, we plot the particle (z, y) positions for both wiggler and PPM configurations, for an initial thin slice of particles starting at the same axial position. They are nearly identical, with slippage <0.1 mm after transport of 10 cm. This small axial slippage will not lead to dephasing of particles for frequencies well in excess of 300 GHz.

In Fig. 7, we show a particle-in-cell (PIC) simulation of the nominal sheet-beam transport in a wiggler field, verifying the PUSHER results, using the PIC code TUBE and simulating the horizontally centered vertical slice as described in reference [13]. For this simulation, 41 000 particles were used in a mesh with 40 vertical divisions and 2400 horizontal divisions.

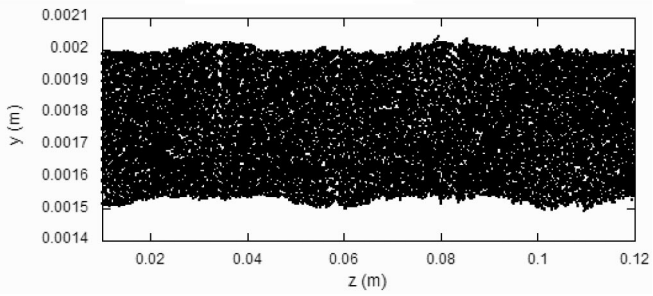

FIG. 7. PIC simulation of the nominal transport in a wiggler field configuration.

VI. NATURAL FOCUSING STABILITY REGIONS FOR WIGGLER AND PPM FIELDS

In this section, we summarize PUSHER simulations of both wiggler and PPM focusing of the nominal sheet beam (1 cm by 0.5 mm), varying the focusing period, for both space-charge and emittance-dominated beams. We will use these calculations to delineate the stability regions for both wiggler and PPM focusing, with both space-charge dominated and emittance-dominated beams. The horizontal space-charge force was neglected in the calculations shown in this section, in order to isolate the natural focusing stability issues.

In the first figure, Fig. 8, we plot the normalized envelope ripple amplitude for both emittance-dominated and space-charge dominated beams with wiggler focusing [in Fig. 8(a)] and with PPM focusing [in Fig. 8(b)]. The normalized ripple amplitude is defined as the peak-to-peak envelope variation, divided by the equilibrium envelope radius. The onset of the instability is sudden. Before the instability, the ripple amplitude evolution is complex, but the ripples reach a maximum size for all the values plotted in Fig. 8. Beyond the stability limit, though, the ripple amplitude does not establish a maximum size, but continually grows without bound as the beam travels down the structure. Note the sudden onset of instability cannot be predicted by the ripple amplitude just below the stability limit, especially for the space-charge dominated case. These calculations all used a magnetic field of 0.209 T, which we found in Sec. IV was the equilibrium focusing strength for an emittance-dominated beam, with a normalized emittance of 1.35 μm. Because the Mathieu α parameter depends on the magnetic field as $\alpha = B_w^2(e/mc\gamma\beta)^2(L/2\pi)^2/2$ [Eq. (22)], the peak field was kept constant for the calculations represented in these plots. To achieve balanced flow for a space-charge dominated beam (with zero emittance), the current was increased to 30.25 A for the 1-cm period. The emittance-dominated case becomes unstable right when the period

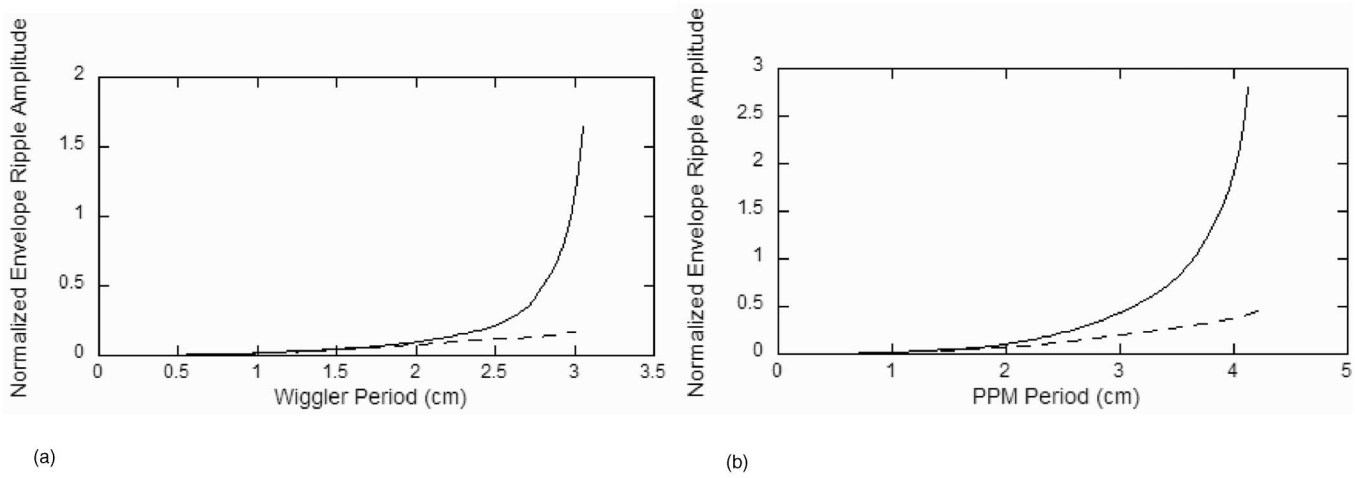

FIG. 8. Envelope ripple amplitude versus focusing period, solid line emittance-dominated beam, dashed space-charge dominated beam. (a) Wiggler focusing. (b) PPM focusing.

reaches at the Mathieu stability boundary of $\alpha = 0.66$, whereas the space-charge dominated case maintains stability a slight bit further. Also as predicted in Sec. III, wiggler focusing leads to unstable flow at a lower α value. However, the onset of the instability is lower than predicted [a 15% decrease in the maximum stable period was predicted from Eq. (24), and about twice that is seen in Fig. 8(a)]. The space-charge dominated beams for both the wiggler and PPM field configurations have significantly lower envelope oscillations than the emittance-dominated beam, for all focusing periods.

Increasing the period for the PPM case did not change the equilibrium emittance or current values, but did for the wiggler period. Because of the large horizontal motion in the wiggle motion, greater average focusing is found for the wiggler case as the period is increased, requiring an increase in the emittance (for the emittance-dominated case) and the current (for the space-charge dominated case) to maintain average balanced flow. The increase in the current and emittance is shown in Fig. 9.

The fractional ripple, for both an emittance-dominated beam in balanced flow and a space-charge dominated beam in balanced flow, for the case of the PPM field configuration [Fig. 8(b)], is replotted as a function of α in Fig. 10, verifying the Mathieu stability limit of $\alpha = 0.66$. (For comparing these figures, $\alpha = 361L^2$, with the period in meters.) This plot can be compared to previously published plots of amplitude ripple due to periodic focusing, which only apply to the space-charge dominated regime [in Refs. [8,9], for example], and which do not show the compromised ripple amplitude of the wiggler focusing configuration.

Figures 8 and 10 are surprising. The space-charge force, which is divergent, suppresses the amplitude of the beam ripple. The onset of total transport instability is right at the Mathieu stability limit of $\alpha = 0.66$ for the emittance-dominated beam, but extends slightly further ($\alpha \sim 0.67$) for the space-charge dominated beam. By counterbalancing the inward magnetic focusing force, the diverging

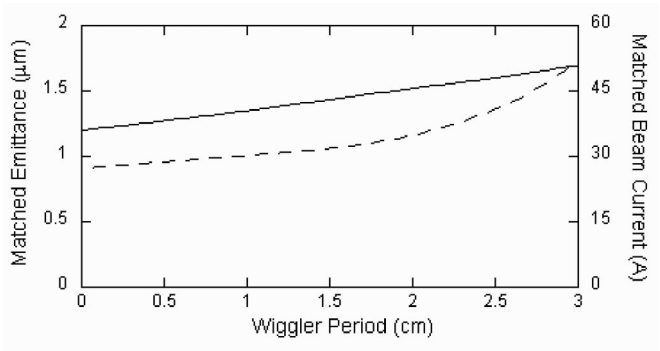

FIG. 9. Increase in normalized emittance (solid line) and current (dashed line) to maintain balanced flow for the emittance and space-charge dominated cases, respectively, as the wiggler period is increased.

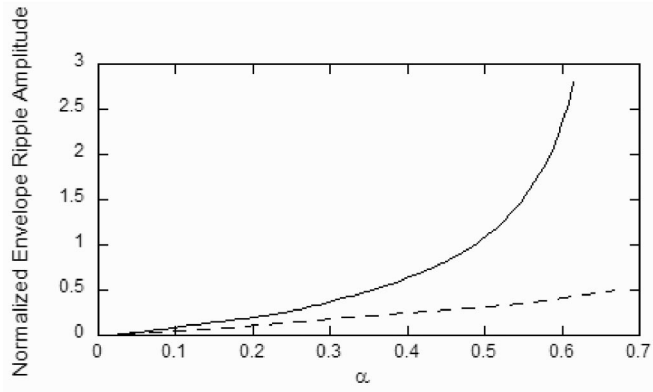

FIG. 10. Fractional ripple as a function of α. The solid line is for the case of an emittance-dominated beam and the dashed line is for the case of a space-charge dominated beam.

space-charge force allows for laminar single-particle orbits that are not possible in an emittance-dominated beam. The increased envelope ripple amplitude near the Mathieu stability limit for the emittance-dominated beam (over a factor of 5 greater, with a ripple amplitude over twice the size of the beam radius itself) has significant consequences for current transmission through these structures. As a general rule, the transport will be better if the equilibrium beam size is made as large as possible as can fit in the structure without interception (typically $\frac{3}{4}$ of the structure size, for microwave tubes). For example, we can compare transport in a structure with the maximum allowable beam radius and with half that radius. With the larger beam radius, the applied magnetic field can be reduced by a factor of 4 as compared to the field required for the smaller radius, and the Mathieu parameter α by a factor of 16 for the same magnet period.

We examine the threshold of the instability for the wiggler case, for both the space-charge dominated beam and the emittance-dominated beam, in Figs. 11 and 12, respectively.

In both cases, the instability is achieved when the normalized relativistic momentum drops below about 0.4. We infer that the decrease in momentum provides enough additional focusing force to effectively reach the thin lens stability limit, which is seen in Figs. 11(c) and 12(c). The greater envelope ripple before instability for the wiggler case is shown in Figs. 11(a) and 12(a), consistent with Figs. 8(a) and 8(b). Also note that the initial envelope oscillation in Fig. 12(a) is relatively small (about 40%). With a slightly longer wiggler period (so the transport is stable in terms of being below the Mathieu threshold), these envelope oscillations grow over distance to about an amplitude of 1.5 mm, and then decrease back down. However, once the stability threshold is crossed, these oscillations continue to grow.

VII. DISCUSSION

Our major conclusions into sheet-beam transport with natural focusing are

(i) A space-charge dominated beam has smaller envelope oscillations than an emittance-dominated beam.

(ii) For natural focusing, the wiggler transport stability threshold is at about $\frac{3}{4}$ that for PPM focusing, in terms of either the peak magnetic field or the focusing period, due to

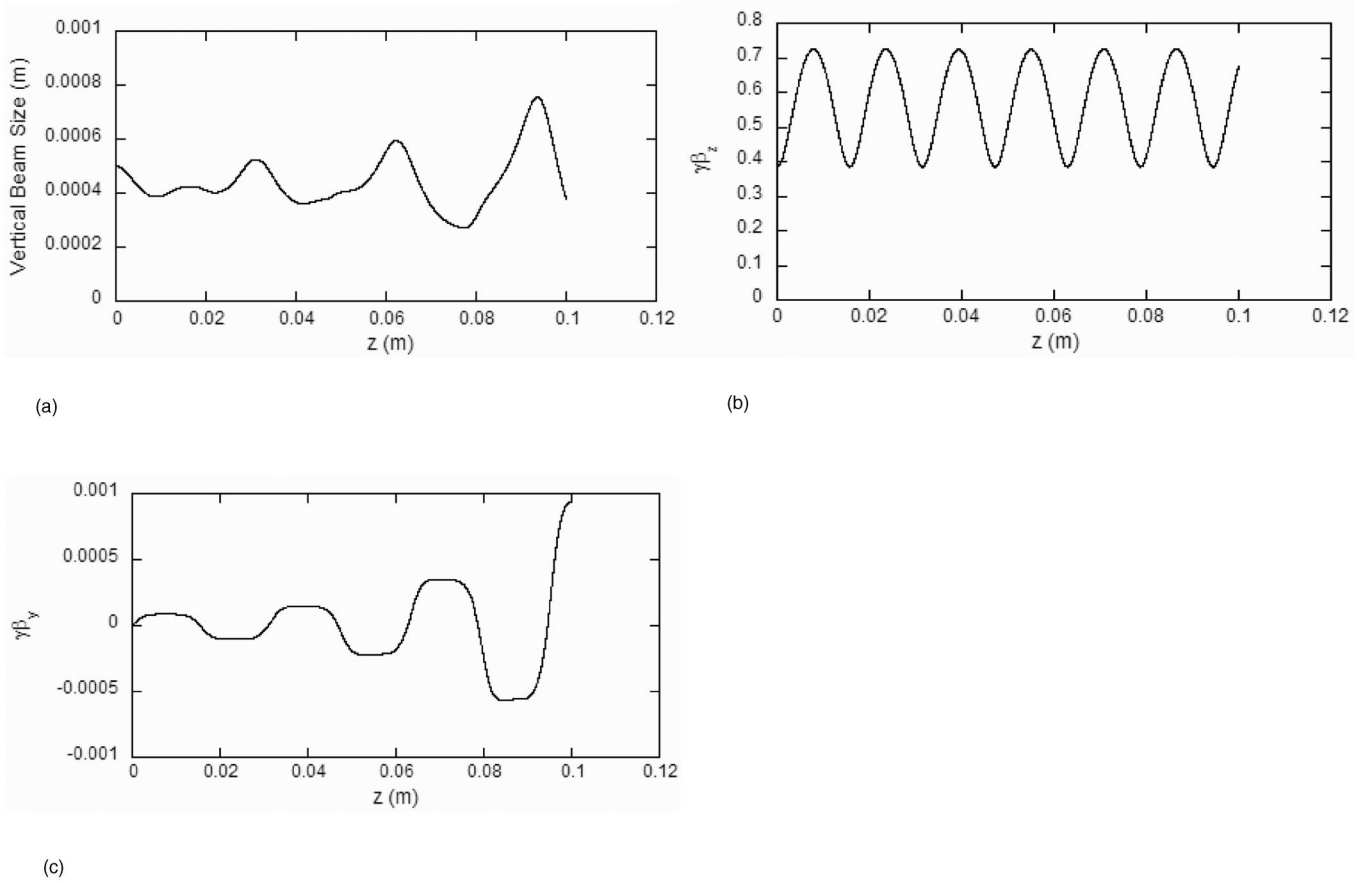

FIG. 11. Instability threshold for wiggler focusing with a space-charge dominated beam, period 3.105 cm. (a) Vertical beam size versus axial position. (b) Longitudinal beam momentum versus axial position. (c) Vertical momentum versus axial position.

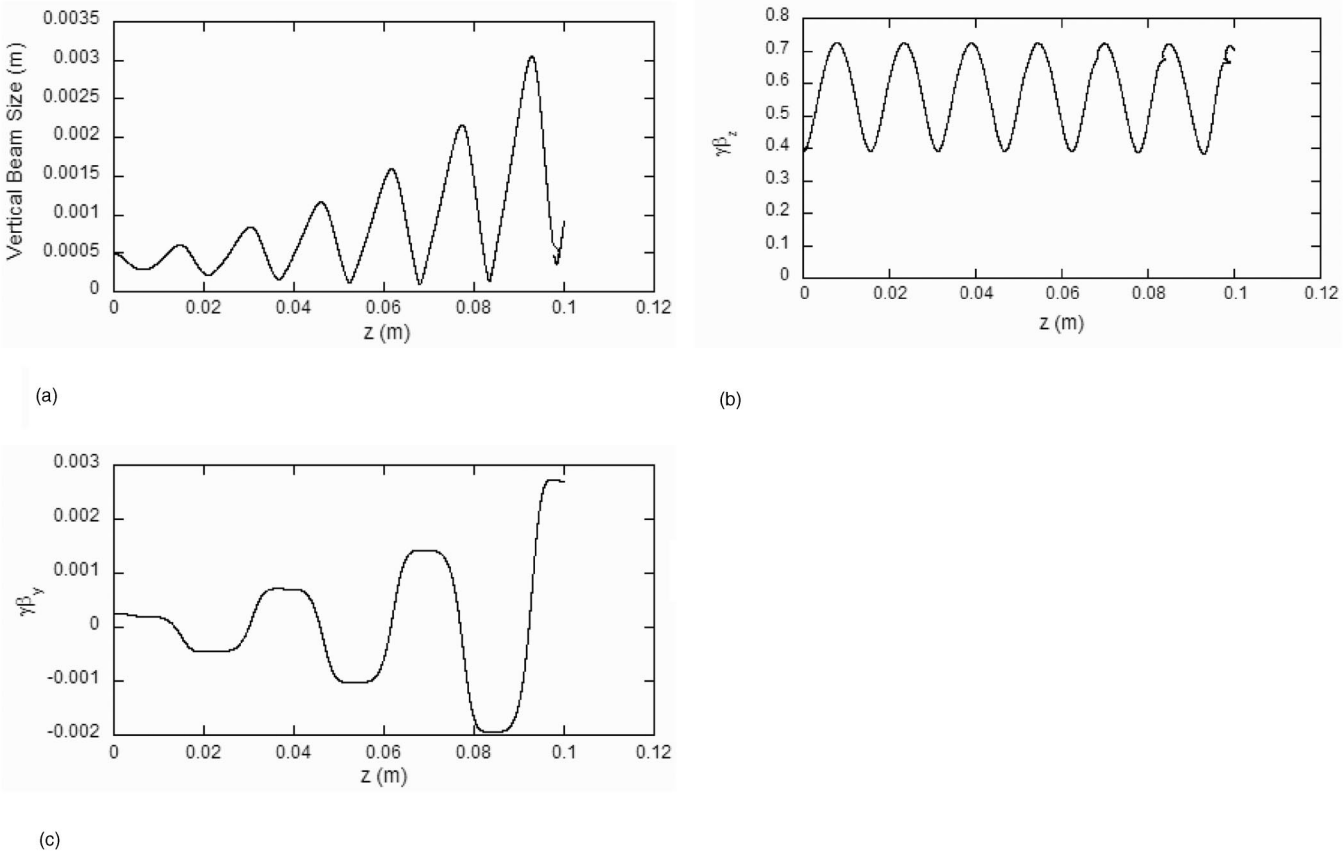

FIG. 12. Instability threshold for wiggler focusing with an emittance-dominated beam, period 3.125 cm. (a) Vertical beam size versus axial position. (b) Longitudinal beam momentum versus axial position. (c) Vertical momentum versus axial position.

unbalanced focusing resulting from the nonparaxial decrease in axial momentum during the wiggler orbits.

The larger envelope oscillations in an emittance-dominated beam is unexpected. We would have expected an emittance-dominated beam to be cleaner, better understood, and overall more stable than a beam with an additional defocusing element. However, this effect appears to be universal, and quite important. The greater laminar flow of a space-charge dominated beam force apparently provides resistance to the instability. Recalling that the Mathieu instability is related to the thin lens overfocusing instability [Eqs. (10)–(12)], it is reasonable to expect this resistance because the overfocusing is reduced as the beam transport becomes more laminar. The beam envelope ripple for an emittance-dominated beam, even below the Mathieu stability limit, can be over 200% of the beam radius, which can significantly impact transport of high-emittance beams in wiggler and PPM structures in terms of potential intercepted current. As was pointed out earlier, for emittance-dominated beams, the maximum beam size can be reduced by actually increasing the equilibrium beam size, if the transport is near the Mathieu stability threshold.

We are also surprised by the larger decrease in stability with wiggler focusing than expected, due to the axial momentum change. PPM focusing appears to be clearly superior, for the case of a circular beam, or an elliptical beam with a modest aspect ratio.

We also predict what happens to the beam emittance if the vertical focusing becomes sufficiently nonlinear. Recalling the envelope equation [Eq. (32)] and the emittance growth equation,

$$\frac{d}{dz}\varepsilon^2 = a\{\langle y^2\rangle\langle y'y''\rangle - \langle yy'\rangle\langle yy''\rangle\} \tag{41}$$

we see that each term in the emittance growth equation is proportional to the emittance for a constant focusing strength. Its solution is then of the form $\varepsilon = \hat{\varepsilon}e^{\hat{\alpha}z}$, so we expect an exponential growth in the emittance due to the nonlinear focusing terms when they become large enough. For our nominal transport parameters, $\hat{\alpha}$ must be very small, as we saw no emittance growth even with a 30% mixing of the PPM and wiggler fields (Figs. 5). However, this coefficient will increase as the transverse dimensions decrease, and may become an issue for very high frequency mm-wave tubes.

ACKNOWLEDGMENTS

This work was supported by funds from the Laboratory-Directed Research and Development program at Los

Alamos National Laboratory, operated by the University of California for the U.S. Department of Energy.

[1] B. E. Carlsten, Phys. Plasmas **9**, 1790 (2002).
[2] B. E. Carlsten, Phys. Plasmas **8**, 4585 (2001).
[3] H. P. Freund and T. M. Abu-Elfadl, IEEE Trans. Plasma Sci. **32**, 1015 (2004).
[4] B. E. Carlsten, Phys. Plasmas **9**, 5088 (2002).
[5] J. H. Booske, B. D. McVey, and T. M. Antonsen, Jr., J. Appl. Phys. **73**, 4140 (1993).
[6] J. H. Booske, M. A. Basten, A. H. Kumbasar, T. M. Antonsen, S. W. Bidwell, Y. Carmel, W. W. Destler, V. L. Granatstein, and D. J. Radack, Phys. Plasmas **1**, 1714 (1994).
[7] M. A. Basten and J. H. Booske, J. Appl. Phys. **85**, 6313 (1999).
[8] J. T. Mendel, C. F. Quate, and W. H. Yocum, Proc. IRE **42**, 800 (1954).
[9] A. S. Gilmour, Jr., *Principles of Traveling-Wave Tubes* (Artech House, Boston, 1994).
[10] Kurt Amboss (private communication).
[11] B. E. Carlsten, S. J. Russell, L. M. Earley, F. Krawczyk, J. M. Potter, P. Ferguson, and S. Humprhies, Jr., IEEE Trans. Plasma Sci. **33**, 85 (2005).
[12] J. D. Lawson, *The Physics of Charged-Particle Beams* (Clarendon Press, Oxford, 1977).
[13] B. E. Carlsten, "Modeling an elliptical sheet beam with a 2½-dimensional particle-in-cell code" (to be published).
[14] C. Birsall and A. Langdon, *Plasma Physics via Computer Simulations* (McGraw-Hill, Inc., New York, 1985).
[15] P. H. Stoltz, J. R. Cary, G. Penn, and J. Wurtele, Phys. Rev. ST Accel. Beams **5**, 094001 (2002).
[16] B. E. Carlsten, L. M. Earley, F. L. Krawczyk, S. J. Russell, J. M. Potter, P. Ferguson, and S. Humphries, Jr., this issue, Phys. Rev. ST Accel. Beams **8**, 062002 (2005).